Progressive memory circuit impairments along with Alzheimer's disease neuropathology spread: evidence from in vivo neuroimaging

Kaicheng Li
the 2nd affiliated hospital of zhejiang university
Shuyue Wang
the 2nd affilaited hospital of zhejiang university
Xiao Luo
the 2nd affiliated hospital of zhejiang university
Qingze Zeng
the 2nd affilaited hospital of zhejiang university
Yerfan Jiaerken
the 2nd affiliated hospital of zhejiang university
Xiaopei Xu
the 2nd affiliated hospital of zhejiang university
Chao Wang
the 2nd affiliated hospital of zhejiang university
Xiaocao Liu
the 2nd affiliated hospital of zhejiang university
Zheyu Li
Zhejiang University
Shuai Zhao
Zhejiang University
Tianyi Zhang
Zhejiang University
Yanv Fu
Zhejiang University
Yanxing Chen
Zhejiang University
Zhirong Liu
the 2nd affiliated hospital of zhejiang university
Jiong Zhou
the 2nd affiliated hospital of zhejiang university
Peiyu Huang

the 2nd affiliated hospital of zhejiang university

Minming Zhang (zhangminming@zju.edu.cn)

Department of Radiology, 2nd Affiliated Hospital of Zhejiang University

---

Research

Keywords: Alzheimer's disease continuum, Tau protein propagation theory, TRACULA, Memory circuit, AT(N) classification system, Hippocampus subfields

Posted Date: February 10th, 2020

DOI: https://doi.org/10.21203/rs.2.23012/v1

Version of Record: A version of this preprint was published at Cerebral Cortex on June 13th, 2020. See the published version at https://doi.org/10.1093/cercor/bhaa162.

Abstract

Background

Along with Alzheimer's disease (AD) continuum, AD neuropathologies propagate trans-neuronally, causing the memory circuit disorganization and memory deficit. However, no evidence supports the hypothesis in vivo to date.

Methods

Based on biological diagnosis criteria, we divided subjects into 5 groups by setting the CSF cutoff point at 192 pg/ml for Aβ 1-42 (A) and 23 pg/ml for P-tau 181 (T): Group 0, cognitively normal (CN) with normal Aβ 1-42 and P-tau 181 (A−T−); Group 1, CN with A+T−; Group 2, CN with A+T+; Group 3, mild cognitive impairments (MCI) with A+T+; Group 4, AD with A+T+. We defined the memory circuit as the hippocampus (HP), cingulum-angular bundles (CAB), and precuneus cortex, respectively representing the starting point, core connecting fiber, and connected downstream cortex. Then we assessed the HP subfields volume, CAB diffusion metric (whole tract-level and waypoint-wise), and precuneus volume. Finally, we correlated neuroimaging measures with cognitive and neuropathological data.

Results

Along AD continuum, HP subfields volume initially increased and then decreased, starting from the early stage (CN with A+T-). CAB integrity loss on both whole tract-level and waypoint-wise in MCI and AD with A+T+ and progressed along AD continuum. Regarding precuneus, we only found the decreased volume in MCI and AD with A+T+, with CN stage spared. Further, memory circuit structure impairment correlated with more AD neuropathology and worse memory profile.

Conclusion

Our results support the tau propagation theory in the memory circuit, suggested that the memory circuit impairments starting from the HP, then propagating to the downstream projection tract and cortex.

Introduction

Alzheimer's disease (AD) is the most common form of dementia, characterized by progressive memory and other cognitive abilities decline. Before the dementia onset, AD neuropathological accumulates for 10–15 years [1] and develops in a specific temporal-ordered pattern [2], with extracellular amyloid-β (Aβ) appears the earliest followed by intracellular phosphorylated tau deposition, and downstream neurodegeneration events [3]. The prior hypothesis shows that these AD neuropathological proteins propagate trans-neuronally and result in neuronal circuit disorganization, especially in the memory circuit, and finally lead to memory loss [4]. Considering the decoupling of clinical symptoms from neuropathological processes, the 2018 NIA-AA also proposed the biological diagnostic framework for AD

[5]. However, it remains unclear that the trajectory of neuronal circuit changes along the biological AD continuum, especially in the memory circuit.

Memory circuit comprises of the hippocampus (HP), the hippocampus-connected white matter fiber pathway (e.g., the cingulum-angular bundles, CAB [6]) and the connected cortex (posterior brain regions) [7]. Notably, HP is composed of several subfields differentially susceptible to AD neuropathology. Previous studies found that HP atrophy is early involved in the face of AD neuropathological deposition, especially the cornu ammonis (CA)1 and subiculum [8] while the downstream cortex impairs later. The possible neuropathological mechanism is the 'misfolded tau protein propagation theory': tau pathology spread through synaptic connectivity and cause the structural impairments [9]. Similar to the Braak stage, tau pathology arises early in the transentorhinal cortex, from where they spread to limbic regions, followed by inferior frontal and parietal cortex [10, 11]. Moreover, the white matter may be the mediation in neuropathology spread, considering that structural tract alterations can predict downstream tau accumulation in amyloid-positive older individuals [12]. The exploration of the memory circuit injury mechanism is expected to provide important clues for further treatment.

Previous microstructural studies have demonstrated the disrupted integrity of the hippocampus-related tract in AD patients [13]. Notably, the cingulum bundle is the region affected most severely, connecting the medial temporal lobe with the posterior cingulate cortex [14–16]. However, prior work only detects the overall white matter disruption but fails to capture the alteration in the conducting ability of the specific impaired WM segments. To better assess tract-level degeneration, we used an establish tract reconstruction technique TRACULA (TRActs Constrained by UnderLying Anatomy). Specifically, TRACULA is a global probabilistic tractography approach, utilizing the underlying anatomic pathways from the fiber tracts atlas of the training datasets and is capable of reconstructing 18 major white matter tracts [17]. An increased number of clinical studies utilized TRACULA and proved its utility and sensitivity in reflecting the specific tract alternations on both whole tract-level and waypoint-wise within the selected pathway [18, 19]. Therefore, TRACULA provides excellent technical support for studying memory circuits.

In the current study, we assessed the impairment pattern of memory circuit along the pathophysiological continuum of AD. Combining the neuropathological hallmarks and symptomatic status, we classified the sample into five profiles to reflect the disease progression along the AD continuum. We used FreeSurfer to segment HP into subfields, and TRACULA to reflect the white matter diffusion metric on both whole tract-level and waypoint-wise within the CAB. Further, the corresponding cortical volume of the CAB connected regions was measured. According to the tau propagation theory, we hypothesized that HP is the first to suffer from AD neuropathology, then followed by the connected tract and downstream cortex.

Methods And Materials

Study participants

The Institutional Review Boards approved our study, and we obtained informed written consent from all subjects at each site. We identified 41 cognitively normal subjects (CN), 56 subjects with mild cognitive impairments (MCI), and 34 AD patients from the ADNI database (Supplementary Material 1, Study participants). Each subject underwent 3D T1 weighted structural scan, DTI scans, cerebrospinal fluid (CSF) assessment, and comprehensive neuropsychological assessments.

Neuropsychological assessment and CSF acquisition

All subjects underwent neuropsychological examinations, including general mental status (MMSE; CDR global and CDR-sob (sum of boxes [20])) and comprehensive memory performance: episodic memory (WMS-LM, immediate and delayed memory; Auditory Verbal Learning Test, AVLT [21, 22]: AVLT 1–5 sum immediate recall, AVLT 6 immediate recall after interference, AVLT 30 min delay recall, AVLT recognition) and semantic memory (Boston Naming Test, BNT; Category fluency).

CSF biomarkers included $A\beta_{1-42}$, total tau (t-tau), and P-tau_{181}, measured by the multiplex xMAP Luminex platform as previously (http://adni.loni.usc.edu/methods/biomarker-analysis/) [23].

Group classifications

The grouping method in this study follows the 2018 NIA-AA research framework (AT(N) system) (Supplementary Material 2). As previous studies reported, we set the CSF cutoff point at 192 pg/ml for $A\beta_{1-42}$ (A) and 23 pg/ml for P-tau_{181} (T) [23, 24]. Subsequently, based on both the biological AT(N) system [5] and cognitive status, we classified all subjects into five groups: (a) Group 0: CN subjects with normal $A\beta_{1-42}$ and P-tau_{181} (A − T−); (b) Group 1: CN subjects with abnormal $A\beta_{1-42}$ and normal P-tau_{181} (A + T−); (c) Group 2: CN subjects with abnormal $A\beta_{1-42}$ and P-tau_{181} (A + T+); (d) Group 3: MCI subjects with abnormal $A\beta_{1-42}$ and P-tau_{181} (A + T+); (e) Group 4: demented subjects with abnormal $A\beta_{1-42}$ and P-tau_{181} (A + T+). Notably, we excluded subjects with normal $A\beta_{1-42}$ and abnormal P-tau_{181} (A-T+) since it was potentially non-AD related pathology [25]. Finally, we included 12 subjects in Group 0, 5 subjects in Group 1, 24 subjects in Group 2, 56 subjects in Group 3, and 34 subjects in Group 4.

MRI acquisition

Based on 3T scanners, T1 weighted images were obtained based on a sagittal volumetric magnetization-prepared rapid gradient-echo (MPRAGE) sequence with the following representative imaging parameters: repetition time (TR) = 2300 ms; echo time (TE) = 3 ms; voxel size = 1.1 × 1.1 × 1.2 mm^3; within plane FOV = 256 × 256 mm^2; flip angle = 9° or 11°. DTI images were obtained with the following imaging parameters: TR = 9000 ms, slice thickness = 2.7 mm, acquisition matrix 256 × 256. Fifty-nine axial slices were acquired without a gap, giving full brain coverage. For each slice, five image without diffusion weighting (b = 0 s/mm^2) and 41 images with diffusion gradients were acquired (b = 1000s/mm^2). More information in the ADNI scanning guide (http://adni.loni.ucla.edu/wp-content/uploads/2010/05/ADNI2_GE_3T_22.0_T2.pdf).

Image Analysis

Brain morphometry

We performed the subcortical segmentation and cortical reconstruction in each subject using “recon-all” processing stream in FreeSurfer version 6.0 (https://surfer.nmr.mgh.harvard.edu/). This process can provide not only grey and white matter segmentation but also surfaces and morphometry data for each subject [26]. Matching of cortical geometry across subjects is performed by registration to a spherical atlas based on individual cortical folding patterns [27]. These anatomic structure segmentation information were further used in the tractography to restrict the probabilistic distribution of the reconstructed pathways.

Correctly, we segmented HP into 24 subfields, including the CA1, CA2/3, CA4, molecular layer, granule-cell molecular layer of the dentate gyrus, subiculum, presubiculum, parasubiculum, fimbria, hippocampus-amygdala-transition-area (HATA), hippocampal fissure, and hippocampal tail in each hemisphere. Then, we used the Bayesian approach to calculate each subfield volume (Fig. 1-A) [28]. Then, estimated intracranial volume (ICV), a proxy for intracranial volume, was calculated to correct the HP subregion for head-size.

Diffusion MRI tractography

Whole-tract diffusion metric analysis

We performed dMRI analysis and tractography using TRACULA, a probabilistic automatic tracking method based on Freesurfer (version 6.0, http://surfer.nmr.mgh.harvard.edu/fswiki) and FSL (https://fsl.fmrib.ox.ac.uk) [17, 29]. In general, the processing details included: (1) structural segmentation: Cortical parcellation and subcortical segmentation were implemented in FreeSurfer. The structure segmentation results, covering the locations and orientations of tracts, were required as anatomical references for tract tracking; (2) pre-processing of DTIs: A standard pre-processing method for DTI, including eddy currents and motion correction, was performed by registering the diffusion-weighting to the b = 0 images. (3) reconstruction: the FSL’s bedpostX algorithm based on a “ball-and-stick” diffusion model was used to calculate the model parameters of each voxel [30]. Finally, the probability distributions for 18 major white matter pathways were generated, including CAB, cingulum-cingulate gyrus (supracallosal) bundle, and uncinate fasciculus (UF).

Participant motion is a confounding factor that may lead to spurious group differences in diffusion MRI [29]. The head motion index computed from the affine registration was evaluated in the TRACULA report [30]. Each subject’s reconstructed tracts underwent a visual inspection, and aberrant or truncated fiber tracts were excluded. Finally, three participants were excluded due to rough translation and rotation.

In this study, we focused on the CAB tract because it connects the HP and angular gyrus and is considered to be an essential pathway in the tau propagation process. Besides, we chose the UF as the reference, considering it connects the medial temporal lobe but not the hippocampus; thus, it has limited

tau accumulation in cognitively intact elderly (Supplementary Material 3) [12, 31]. Regarding the white matter metrics, we extracted the average values of mean diffusivity (MD), fractional anisotropy (FA), axial diffusivity (DA), and radial diffusivity (DR) on both whole tract-level and waypoint-wise within the tract (Fig. 1-B).

Waypoint-wise diffusion metric analysis

To examine the damage pattern of white matter fiber, we further performed the waypoint-wise analysis. The diffusion metric was obtained from multiple contiguous cross-sections along the reconstructed pathway of each subject [32].

Specifically, TRACULA yields a 1D sequence of values for each of DTI measures, consisting of 40–60 comparison points in each tract, computed in the native space of each subject. Correspondence of points between these sequences from different subjects is established by aligning the mid-points of the sequences. We used sequences for point-wise analyses along the trajectory of a specific pathway.

Tract connected cortical regions volume analysis

To explore the downstream cortical volume changes along with AD progress, we extracted the volume of cortical regions, where the selected tract connected, from the Freesurfer structure segmentation results. Here, we chose the bilateral precuneus as cortical ROIs considering its connection with temporal structures through CAB [33]. We extracted the cortical ROIs volume and normalized it to ICV for statistical analyses (Fig. 1-C).

Statistical analysis

Based on SPSS software (Version 19), we analyzed the demographic data using the Chi-squared test for categorical data (gender, APOE ε4 status) and t-test for continuous data (age, education, and GDS) (Table 1, Supplementary Material 4). Regarding the brain morphometry, we examined the difference between HP subfields and the bilateral precuneus between groups by using the two-sample t-test.

Table 1

Demographic and neuropsychological data in subjects along with the AD continuum

Demographic characteristics	Group 0 N = 12	Group 1 N = 5	Group 2 N = 24	Group 3 N = 56	Group4 N = 34	P-value
Age, y, mean (SD)	73.21 ± 5.41	72.72 ± 5.87	76.27 ± 5.95	74.14 ± 7.52	74.11 ± 8.95	G1-G0 = 0.87
						G2-G0 = 0.14
						G3-G0 = 0.69
						G4-G0 = 0.68
Female, n (%)	6 (50.00%)	3 (60.00%)	17 (70.83%)	22 (39.29%)	14 (41.18%)	G1-G0 = 0.56
						G2-G0 = 0.20
						G3-G0 = 0.36
						G4-G0 = 0.42
Education, y, mean (SD)	17.67 ± 1.87	15.00 ± 2.24	16.00 ± 2.27	15.50 ± 2.74	15.12 ± 2.78	G1-G0 = 0.02*
						G2-G0 = 0.04*
						G3-G0 = 0.003*
						G4-G0 = 0.005*
APOE ε4 status, n (%)	1 (8.33%)	2 (40.00%)	12 (50.00%)	40 (71.43%)	24 (70.59%)	G1-G0 = 0.19
						G2-G0 = 0.02*

Data are presented as means ± standard deviations. * P < 0.05.

Abbreviation: A: Aβ1–42; T: P-tau181; Group 0: cognitively normal subjects with A − T−; Group 1: cognitively normal subjects with A + T−; Group 2: cognitively normal subjects with A + T+; Group 3: mild cognitive impairment subjects with A + T+; Group 4: demented subjects with A + T+; GDS: Geriatric Depression Scale; MMSE, Mini-Mental State Examination; CDR: Clinical Dementia Rating; WMS-LM, Wechsler Memory Scale Logical Memory; AVLT, Auditory Verbal Learning Test; BNT, Boston Naming Test. AvgTranslation: average translation; AvgRotation: average rotation

Demographic characteristics	Group 0 N = 12	Group 1 N = 5	Group 2 N = 24	Group 3 N = 56	Group4 N = 34	P-value
						G3-G0 < 0.001*
						G4-G0 < 0.001*
GDS	1.25 ± 1.22	0.60 ± 0.55	0.88 ± 1.48	1.68 ± 1.42	1.88 ± 1.41	G1-G0 = 0.28
						G2-G0 = 0.46
						G3-G0 = 0.33
						G4-G0 = 0.17
General mental status						
MMSE	28.50 ± 2.02	29.20 ± 0.84	28.67 ± 1.40	27.41 ± 1.79	23.03 ± 2.28	G1-G0 = 0.47
						G2-G0 = 0.77
						G3-G0 = 0.07
						G4-G0 < 0.001*
CDR global	0.00 ± 0.00	0.00 ± 0.00	0.00 ± 0.00	0.50 ± 0.00	0.79 ± 0.25	/
						/
						/
						G4-G0 < 0.001*
CDR sum	0.13 ± 0.23	0.10 ± 0.22	0.04 ± 0.14	1.45 ± 0.92	4.63 ± 1.52	G1-G0 = 0.84

Data are presented as means ± standard deviations. * P < 0.05.

Abbreviation: A: Aβ1−42; T: P-tau181; Group 0: cognitively normal subjects with A − T−; Group 1: cognitively normal subjects with A + T−; Group 2: cognitively normal subjects with A + T+; Group 3: mild cognitive impairment subjects with A + T+; Group 4: demented subjects with A + T+; GDS: Geriatric Depression Scale; MMSE, Mini-Mental State Examination; CDR: Clinical Dementia Rating; WMS-LM, Wechsler Memory Scale Logical Memory; AVLT, Auditory Verbal Learning Test; BNT, Boston Naming Test. AvgTranslation: average translation; AvgRotation: average rotation

Demographic characteristics	Group 0 N = 12	Group 1 N = 5	Group 2 N = 24	Group 3 N = 56	Group4 N = 34	P-value
						G2-G0 = 0.26
						G3-G0 < 0.001*
						G4-G0 < 0.001*
Episodic Memory						
WMS-LM immediate	14.17 ± 2.92	10.80 ± 3.83	13.22 ± 3.83	8.25 ± 3.80	3.24 ± 1.86	G1-G0 = 0.07
						G2-G0 = 0.46
						G3-G0 < 0.001*
						G4-G0 < 0.001*
WMS-LM delay	11.92 ± 2.15	9.60 ± 2.88	12.39 ± 3.58	5.77 ± 4.11	1.35 ± 1.59	G1-G0 = 0.09
						G2-G0 = 0.68
						G3-G0 < 0.001*
						G4-G0 < 0.001*
AVLT sum of trials 1–5	46.42 ± 10.89	46.00 ± 13.02	46.04 ± 8.32	32.21 ± 8.83	20.94 ± 6.77	G1-G0 = 0.95
						G2-G0 = 0.91
						G3-G0 < 0.001*

Data are presented as means ± standard deviations. * P < 0.05.

Abbreviation: A: Aβ1–42; T: P-tau181; Group 0: cognitively normal subjects with A − T−; Group 1: cognitively normal subjects with A + T−; Group 2: cognitively normal subjects with A + T+; Group 3: mild cognitive impairment subjects with A + T+; Group 4: demented subjects with A + T+; GDS: Geriatric Depression Scale; MMSE, Mini-Mental State Examination; CDR: Clinical Dementia Rating; WMS-LM, Wechsler Memory Scale Logical Memory; AVLT, Auditory Verbal Learning Test; BNT, Boston Naming Test. AvgTranslation: average translation; AvgRotation: average rotation

Demographic characteristics	Group 0 N = 12	Group 1 N = 5	Group 2 N = 24	Group 3 N = 56	Group4 N = 34	P-value
						G4-G0 < 0.001*
AVLT6 (immediate Recall)	8.08 ± 3.65	9.80 ± 4.32	9.04 ± 3.52	4.46 ± 3.02	1.47 ± 1.56	G1-G0 = 0.42
						G2-G0 = 045
						G3-G0 = 0.001*
						G4-G0 < 0.001*
AVLT30min (Delay Recall)	7.00 ± 4.51	8.60 ± 4.39	7.50 ± 4.11	3.29 ± 3.45	0.59 ± 1.18	G1-G0 = 0.51
						G2-G0 = 0.74
						G3-G0 = 002*
						G4-G0 < 0.001*
AVLT recognition (recognition)	11.67 ± 3.14	14.40 ± 0.55	12.75 ± 2.38	10.71 ± 3.14	6.56 ± 3.98	G1-G0 = 0.01*
						G2-G0 = 0.26
						G3-G0 = 0.34
						G4-G0 < 0.001*
Semantic Memory						
BNT	28.67 ± 1.50	27.00 ± 2.55	27.50 ± 2.55	25.98 ± 3.48	20.94 ± 5.68	G1-G0 = 0.11

Data are presented as means ± standard deviations. * P < 0.05.

Abbreviation: A: Aβ1−42; T: P-tau181; Group 0: cognitively normal subjects with A − T−; Group 1: cognitively normal subjects with A + T−; Group 2: cognitively normal subjects with A + T+; Group 3: mild cognitive impairment subjects with A + T+; Group 4: demented subjects with A + T+; GDS: Geriatric Depression Scale; MMSE, Mini-Mental State Examination; CDR: Clinical Dementia Rating; WMS-LM, Wechsler Memory Scale Logical Memory; AVLT, Auditory Verbal Learning Test; BNT, Boston Naming Test. AvgTranslation: average translation; AvgRotation: average rotation

Demographic characteristics	Group 0 N = 12	Group 1 N = 5	Group 2 N = 24	Group 3 N = 56	Group4 N = 34	P-value
						G2-G0 = 0.09
						G3-G0 < 0.001*
						G4-G0 < 0.001*
Category fluency	21.58 ± 5.74	18.60 ± 5.50	21.83 ± 4.90	16.73 ± 5.32	12.00 ± 5.20	G1-G0 = 0.34
						G2-G0 = 0.89
						G3-G0 = 0.006*
						G4-G0 < 0.001*
CSF						
$A\beta_{1-42}$ (pg/ml)	230.58 ± 20.34	160.6 ± 28.17	143.64 ± 24.22	136.30 ± 20.34	128.89 ± 22.00	G1-G0 < 0.001*
						G2-G0 < 0.001*
						G3-G0 < 0.001*
						G4-G0 < 0.001*
T-Tau (pg/ml)	46.49 ± 9.21	37.54 ± 17.06	85.38 ± 33.00	112.13 ± 64.99	139.34 ± 64.19	G1-G0 = 0.18
						G2-G0 < 0.001*
						G3-G0 < 0.001*

Data are presented as means ± standard deviations. * P < 0.05.

Abbreviation: A: Aβ1−42; T: P-tau181; Group 0: cognitively normal subjects with A − T−; Group 1: cognitively normal subjects with A + T−; Group 2: cognitively normal subjects with A + T+; Group 3: mild cognitive impairment subjects with A + T+; Group 4: demented subjects with A + T+; GDS: Geriatric Depression Scale; MMSE, Mini-Mental State Examination; CDR: Clinical Dementia Rating; WMS-LM, Wechsler Memory Scale Logical Memory; AVLT, Auditory Verbal Learning Test; BNT, Boston Naming Test. AvgTranslation: average translation; AvgRotation: average rotation

Demographic characteristics	Group 0 N = 12	Group 1 N = 5	Group 2 N = 24	Group 3 N = 56	Group4 N = 34	P-value
						G4-G0 < 0.001*
P-Tau$_{181}$ (pg/ml)	18.96 ± 2.69	16.72 ± 4.70	49.43 ± 26.43	55.88 ± 25.04	66.97 ± 39.82	G1-G0 = 0.36
						G2-G0 < 0.001*
						G3-G0 < 0.001*
						G4-G0 < 0.001*
Head Motion						
AvgTranslation	1.54 ± 0.69	1.49 ± 0.60	1.32 ± 0.65	1.58 ± 0.50	1.33 ± 0.56	G1-G0 = 0.90
						G2-G0 = 0.34
						G3-G0 = 0.77
						G4-G0 = 0.30
AvgRotation	0.007 ± 0.003	0.009 ± 0.005	0.006 ± 0.002	0.007 ± 0.003	0.006 ± 0.002	G1-G0 = 0.54
						G2-G0 = 0.06
						G3-G0 = 0.43
						G4-G0 = 0.19
Data are presented as means ± standard deviations. * P < 0.05.						
Abbreviation: A: Aβ1−42; T: P-tau181; Group 0: cognitively normal subjects with A − T−; Group 1: cognitively normal subjects with A + T−; Group 2: cognitively normal subjects with A + T+; Group 3: mild cognitive impairment subjects with A + T+; Group 4: demented subjects with A + T+; GDS: Geriatric Depression Scale; MMSE, Mini-Mental State Examination; CDR: Clinical Dementia Rating; WMS-LM, Wechsler Memory Scale Logical Memory; AVLT, Auditory Verbal Learning Test; BNT, Boston Naming Test. AvgTranslation: average translation; AvgRotation: average rotation						

Regarding the DTI results, we focused on the bilateral CAB and analyzed white matter microstructural disruptions on both whole tract-level and waypoint-wise. Firstly, tract-level significance tests were

performed using general linear models (GLM): mean FA, MD, DR, and DA of the whole WM tract as the dependent variable; group as a categorical predictor, age, gender, and education as co-variables. Then, we assessed the waypoint-wise significance for each 2.7 mm segment by using GLMs: FA, MD, DR, and DA of each segment as the dependent variable; group as a categorical predictor, age, gender, education, and the selected tract volume as the co-variables. To reduce the false-positive rate, we reported the results only if they showed a significant group difference ($p < 0.05$) over contiguous segments greater than 0.81 cm along a chosen pathway [32].

We defined brain structural regions showing significant between-group differences as ROIs and extracted the averaged values. Then, across all subjects, we correlated memory circuit (including HP subfields volume and the diffusion metrics of CAB tract) with memory ability through the linear regression analyses controlled for age, gender, and education. Furthermore, across all subjects, we conducted Pearson correlation analysis between the memory circuit and AD neuropathology to explore the possible mechanism.

Results

HP subfields volume

As the AD neuropathology progress, the extent of HP atrophy gradually increases. Specifically, relatively to Group 0, patients in Group 1 had larger right presubiculum ($p = 0.03$) and parasubiculum ($p = 0.027$); Group 2 had smaller CA1 ($p = 0.048$); Group 3 and Group 4 had widespread decreased HP subfields volume (Fig. 2; Supplementary material 5, Table s4 and Figure s2).

Whole-tract diffusion metrics

Regarding the left CAB, Group 4 showed increased DA, DR and MD compared to group 0. Regarding the right CAB, Group 3 showed increased DA when compared to Group 0, and Group 4 showed increased DA and MD compared to group 0 (Fig. 3; Supplementary material 5, Table s5 and s6).

Waypoint-wise diffusion metrics analysis

Similar diffusion profiles could be observed in 5 groups, while the WM diffusivity at the late stage of AD showed a distinct variation compared to CN (Fig. 4).

Specifically, compared to Group 0, Group 1 showed significantly lower FA and higher MD in 0.81 cm long segments on the left CAB. Group 2 showed a significantly increased DA in a 1.35 cm long segment in the central portion of the left CAB. Group 3 showed two increased DA segments over 0.81 cm long in the central and posterior portion of left CAB, and one increased MD segment in the posterior portion of left CAB; one increased DA segment in the central portion of right CAB. Group 4 showed a significant increased DA in a 0.81 cm long segment in the central portion of left CAB, and a significant increased MD and DR in a 0.81 cm long segment in the central portion of left CAB (Fig. 5).

Tract connected cortical regions volume analysis

Compared to Group 0, Group 3 showed decreased volume in the left precuneus;

Group 4 showed decreased volume in the bilateral precuneus. No significant difference was found in Group 2 and Group 1 when compared to Group 0 (Fig. 6).

Relationship between the memory circuit integrity, memory, and AD neuropathology
Linear regression analyses showed the positive association between HP subfields and memory, including the parasubiculum, subiculum, CA1, molecular layer, and et al. As for the CAB tract, DR and MD showed a negative association with memory (Supplementary material 6).

Pearson correlation showed that HP subfield positively correlated with the Aβ, but negatively correlated with tau. As for the CAB tract, DR and MD showed a negative correlation between Aβ (Supplementary Material 7).

Notably, to show the progressive pattern of the memory circuit, we also performed a comparison between groups 1, 2, 3, and 4 (Supplementary material 8). Finally, to show the results more clearly, we gathered all results in Fig. 7 to show the progressive impairments of memory circuit structure along with AD neuropathology spread.

Discussion

This study explored the progressive impairments of memory circuit structure as the AD neuropathological deposition increases: initially, atrophy appears in HP subfields, followed by the CAB impairments and the downstream brain cortex atrophy. Our study supported the AD neuropathology spread theory in the memory circuit in vivo, especially the tau propagation theory, and might conducive to the development of therapeutic methods.

The diphasic trajectory change of HP subfields volume along progressive AD neuropathology

As the core memory-related region, HP comprises subfields with different functions, connecting to other brain regions with different susceptibility to AD-related pathologies. Previous studies regarded HP as the most robust and sensitive biomarker of AD [34]. In line with expectations, our results showed that HP subfields volume had initially increased and then decreased along the AD continuum. To be specific, HP subfields volume showed an initial increase in CN with A + T-, then a decrease in CN with A + T + and progressive decrease with AD neuropathology progress (MCI with A + T + and AD with A + T+).

Our findings are consistent with previous work, documenting that increased HP subfields volume in subjects with abnormal Aβ and then decreased the volume in subjects with both abnormal tau and Aβ [7, 35]. The possible mechanism may be the initial compensation resulted by Aβ, while strengthened impairments resulted from the simultaneous presence of both tau and Aβ [7]. Our results also supported this hypothesis. Firstly, the earliest involved HP subfields in our study include the presubiculum, parasubiculum and CA1. This spatial signature of HP subfields is consistent with the Braak staging of tau pathology: neurofibrillary tangles seed in the entorhinal cortex and then spread to CA1 and subiculum [10]. Further, our correlation analysis showed that increased Aβ linked with increased HP subfields in CN

with A + T-, while increased tau linked with HP subfields atrophy in CN with A + T+. These results suggested that the concurrent presence of Aβ and tau is the tipping point of HP atrophy. Then, HP tends to show a progressive decrease with AD neuropathology develops.

CAB integrity started to impair from the MCI stage and then accelerated with the development of AD neuropathology

White matter damage plays a pivotal role in AD onset and progression. The underlying mechanism may involve in the demyelination, microglial activation, oligodendrocytes loss and reactive astrocytosis in the WM microstructure [36]. Thereinto, CAB carries hippocampal projections to the medial parietal lobe and acts as the most affected white matter tract by AD neuropathology.

Our study focused on the CAB tract and found its microstructural integrity disrupted on both whole-tract level and waypoint-wise along AD neuropathology. To be specific, our tract-based analysis showed impaired CAB integrity in AD and MCI with A + T+. Similarly, previous studies reported the CAB impairments in MCI and AD patients [13]. The possible mechanism may be the spread of tau pathology. One study found the association between the tau pathology and DTI alternations in AD, especially involving the medial temporal limbic connections and medial parietal white matter [37]. Similarly, the work of Lee et al. also found that the deterioration of fiber is the most important place for fiber loss is where it connects to medial temporal lobe regions [13]. On the other hand, our study observed that no significant difference in UF, which was not involved in the tau spread through HP-connected white matter tracts [12].

Furthermore, our waypoint-wise analysis on CAB also showed a dynamic WM change as AD neuropathological developing, starting from the middle of CAB, subsequently expanding to the posterior cerebral region, mainly reflected by DA metric. These results suggested that Wallerian degeneration from the upstream GM atrophy might be the main mechanism. Moreover, CAB has connections to HP, which was affected early by the AD pathology, including the tau pathology. Thus, we inferred that the tau propagation along the tract might cause the CAB impairments.

Notably, our study found that WM impairment appeared in MCI and AD, with the CN stage spared. Our waypoint-wise analysis showed similar diffusion profiles in the CN, early and middle AD stages, while variated diffusivity in the final stage. These findings may suggest that the WM tract gets involved at the relatively late stage of AD. Similarly, another study of nondemented older adults also reported that decreased FA only in those who also had grey matter atrophy and hypometabolism [38]. The possible mechanism may be that having abnormal Aβ, without upstream GM neurodegeneration, was not sufficient for the impaired integrity of the WM tract.

Tract connected cortical regions volume changes at the relatively late stage of AD

As the tract connected cortical region, the precuneus is one of the critical regions in AD and associated with cognition [39]. Our results showed decreased precuneus volume only in MCI and AD with A + T+, but not in other groups. These results suggested that the downstream brain cortex affected until the late

stage. One possible mechanism is the tau pathology spread along the memory circuit. Also, Jacobs et al. found that HP cingulum bundle diffusivity could predict the tau accumulation in the downstream-connected posterior cingulate cortex in subjects with A+ [12]. Another possible mechanism may be that neuronal loss appears to be axonal degeneration, with anterograde (Wallerian, trans-synaptic) effects leading to secondary grey matter degeneration in the downstream cortex [40]. For example, one study focusing on the preterm also found that downstream GM may be affected by aberrant white matter structure [32].
Conclusion: Memory circuit damage pattern and potential mechanism

Our study results showed a progressively structural impairment pattern of memory circuit with the development of AD neuropathology: starting from the upstream GM, then leading to the deterioration of CAB, and the downstream GM atrophy. Thereinto, Aβ and tau pathology are the trigger of the memory circuit impairment, including the GM volume and white matter integrity. Besides, the WM impairments at the stage of AD might be caused by Wallerian degeneration from the upstream GM atrophy and progress due to tau propagation along the tract. Such structural impairments may lead to progressive memory loss in subjects along AD continuum. These results agreed and extended several previous works that found that tau pathology propagation, facilitated by amyloid pathology, may occur along connected pathways [12, 13] and affects the white matter tracts connecting the hippocampus with the distal region [9]. Our work may be conducive to the development of therapeutic methods.

Limitations

Firstly, our study is cross-sectional research, so we unable to explore the casual relationship between HP subfields, WM tract integrity and precuneus volume. Although we try to use the subjects with different disease stages to simulate the AD continuum, further study with exact longitudinal data is needed. Moreover, the sample size of CN with A + T- is relatively small, which may weaken the statistical effort. Further study with a bigger sample size should be performed. Finally, TRACULA is unable to reconstruct other fibers like fornix, the further study which combined several methods should be performed.

Declarations

Ethics approval and consent to participate

All procedures performed in studies involving human participants were in accordance with the ethical standards of the institutional and national research committee and with the 1964 Helsinki declaration and its later amendments or comparable ethical standards. Written informed consent was obtained from all participants and authorized representatives, and the study partners before any protocol-specific procedures were carried out in the ADNI study. More details in http://www.adni-info.org.

Consent for publication

Not applicable

Availability of data and material

The datasets generated and analyzed during the current study are available in the ADNI study. More details in www.adni-info.org.

Competing interests

† Kaicheng Li, Shuyue Wang and Xiao Luo contributed equally to this work. The authors declare no conflict of interest.

Funding

This study was funded by the National Natural Science Foundation of China (Grant No. 81901707) and National Key Research and Development Program of China (Grant No. 2016YFC1306600).

Authors' contributions

KL, SW, XL contributed equally to this work. KL designed the study and wrote the first draft of the manuscript. SW, JY, XX analysed the MRI data and wrote the protocol. XL, QZ, LX, LZ, ZS and ZT, FY collected clinical and MRI data. JZ, CW, CY, LZ, PH, and MZ assisted with study design and interpretation of findings. All authors have contributed to and approved the final manuscript.

All authors read and approved the final manuscript.

Acknowledgement

Not applicable

References

[1] Villemagne V. L., Burnham S., Bourgeat P., Brown B., Ellis K. A., Salvado O., Szoeke C., Macaulay S. L., Martins R., Maruff P., Ames D., Rowe C. C., Masters C. L., Australian Imaging Biomarkers, Lifestyle Research Group (2013) Amyloid beta deposition, neurodegeneration, and cognitive decline in sporadic Alzheimer's disease: a prospective cohort study. *Lancet Neurol* **12**, 357-367.

[2] Sperling R., Mormino E., Johnson K. (2014) The evolution of preclinical Alzheimer's disease: implications for prevention trials. *Neuron* **84**, 608-622.

[3] Jack C. R., Jr., Knopman D. S., Jagust W. J., Petersen R. C., Weiner M. W., Aisen P. S., Shaw L. M., Vemuri P., Wiste H. J., Weigand S. D., Lesnick T. G., Pankratz V. S., Donohue M. C., Trojanowski J. Q. (2013) Tracking pathophysiological processes in Alzheimer's disease: an updated hypothetical model of dynamic biomarkers. *Lancet Neurol* **12**, 207-216.

[4] Myers N., Pasquini L., Gottler J., Grimmer T., Koch K., Ortner M., Neitzel J., Muhlau M., Forster S., Kurz A., Forstl H., Zimmer C., Wohlschlager A. M., Riedl V., Drzezga A., Sorg C. (2014) Within-patient correspondence of amyloid-beta and intrinsic network connectivity in Alzheimer's disease. *Brain* **137**, 2052-2064.

[5] Jack C. R., Jr., Bennett D. A., Blennow K., Carrillo M. C., Dunn B., Haeberlein S. B., Holtzman D. M., Jagust W., Jessen F., Karlawish J., Liu E., Molinuevo J. L., Montine T., Phelps C., Rankin K. P., Rowe C. C., Scheltens P., Siemers E., Snyder H. M., Sperling R., Contributors (2018) NIA-AA Research Framework: Toward a biological definition of Alzheimer's disease. *Alzheimers Dement* **14**, 535-562.

[6] Heilbronner SR Haber SN (2014) Frontal cortical and subcortical projections provide a basis for segmenting the cingulum bundle: implications for neuroimaging and psychiatric disorders. *J Neurosci* **34**, 10041-10054.

[7] Tardif CL Devenyi GA, Amaral RSC, Pelleieux S, Poirier J, Rosa-Neto P, Breitner J, Chakravarty MM; PREVENT-AD Research Group (2018) Regionally specific changes in the hippocampal circuitry accompany progression of cerebrospinal fluid biomarkers in preclinical Alzheimer's disease. *Hum Brain Mapp* **39**, 971-984.

[8] Wang L., Fagan, A. M., Shah, A. R., Beg, M. F., Csernansky, J. G., Morris, J. C., & Holtzman, D. M (2012) Cerebrospinal fluid proteins predict longitudinal hippocampal degeneration in early-stage dementia of the Alzheimer type. *Alzheimer Disease & Associated Disorders* **26**, 314–321.

[9] Ahmed Z Cooper J, Murray TK, Garn K, McNaughton E, Clarke H, Parhizkar S, Ward MA, Cavallini A, Jackson S, Bose S, Clavaguera F, Tolnay M, Lavenir I, Goedert M, Hutton ML, O'Neill MJ (2014) A novel in vivo model of tau propagation with rapid and progressive neurofibrillary tangle pathology: the pattern of spread is determined by connectivity, not proximity. *Acta Neuropathologica* **127**, 667-683.

[10] Braak H Braak E (1991) Neuropathological staging of Alzheimer-related changes. *Acta Neuropathologica* **82**, 239–259.

[11] Braak H Braak E (1995) Staging of Alzheimer’s disease-related neurofibrillary changes. *Neurobiol Aging* **16**, 271–278.

[12] Jacobs HIL Hedden T, Schultz AP, Sepulcre J, Perea RD, Amariglio RE, Papp KV, Rentz DM, Sperling RA, Johnson KA (2018) Structural tract alterations predict downstream tau accumulation in amyloid-positive older individuals. *Nat Neurosci* **21**, 424-431.

[13] Lee SH Coutu JP, Wilkens P, Yendiki A, Rosas HD, Salat DH; Alzheimer’s disease Neuroimaging Initiative (ADNI) (2015) Tract-based analysis of white matter degeneration in Alzheimer's disease. *Neuroscience* **301**, 79-89.

[14] Catani M., & De Schotten, M. T (2008) A diffusion tensor imaging tractography atlas for virtual in vivo dissections. *Cortex* **44**, 1105–1132.

[15] Hua K., Zhang, J., Wakana, S., Jiang, H., Li, X., Reich, D. S., Calabresi, P. A., Pekar, J. J., van Zijl, P. C., & Mori, S (2008) Tract probability maps in stereotaxic spaces: analyses of white matter anatomy and tract-specific quantification. *NeuroImage* **39**, 336–347.

[16] Lin Y. C., Shih, Y. C., Tseng, W. Y., Chu, Y. H., Wu, M. T., Chen, T. F., Tang, P. F., & Chiu, M. J (2014) Cingulum correlates of cognitive functions in patients with mild cognitive impairment and early Alzheimer's disease: a diffusion spectrum imaging study. *Brain Topography* **27**, 393–402.

[17] Yendiki A Panneck P, Srinivasan P, Stevens A, Zöllei L, Augustinack J, Wang R, Salat D, Ehrlich S, Behrens T, Jbabdi S, Gollub R, Fischl B (2011) Automated probabilistic reconstruction of white-matter pathways in health and disease using an atlas of the underlying anatomy. *Front Neuroinform* **5**, 23.

[18] Watanabe A Nakamae T, Sakai Y, Nishida S, Abe Y, Yamada K, Yokota I, Narumoto J (2018) The detection of white matter alterations in obsessive-compulsive disorder revealed by TRActs Constrained by UnderLying Anatomy (TRACULA). *Neuropsychiatr Dis Treat* **14**, 1635-1643.

[19] Pietracupa S Suppa A, Upadhyay N, Giannì C, Grillea G, Leodori G, Modugno N, Di Biasio F, Zampogna A, Colonnese C, Berardelli A, Pantano P (2018) Freezing of gait in Parkinson's disease: gray and white matter abnormalities. *J Neurol* **265**, 52-62.

[20] O'Bryant SE Waring SC, Cullum CM, Hall J, Lacritz L, Massman PJ, Lupo PJ, Reisch JS, Doody R; Texas Alzheimer's Research Consortium (2008) Staging dementia using Clinical Dementia Rating Scale Sum of Boxes scores: a Texas Alzheimer's research consortium study. *Arch Neurol* **65**, 1091-1095.

[21] Geffen GM Butterworth P, Geffen LB (1994) Test-retest reliability of a new form of the auditory verbal learning test (AVLT). *Arch Clin Neuropsychol* **9**, 303-316.

[22] Moradi E Hallikainen I, Hänninen T, Tohka J; Alzheimer's Disease Neuroimaging Initiative (2016) Rey's Auditory Verbal Learning Test scores can be predicted from whole brain MRI in Alzheimer's disease. *Neuroimage Clin* **13**, 415-427.

[23] Shaw L. M., Vanderstichele H., Knapik-Czajka M., Clark C. M., Aisen P. S., Petersen R. C., Blennow K., Soares H., Simon A., Lewczuk P., Dean R., Siemers E., Potter W., Lee V. M., Trojanowski J. Q., Alzheimer's Disease Neuroimaging Initiative (2009) Cerebrospinal fluid biomarker signature in Alzheimer's disease neuroimaging initiative subjects. *Ann Neurol* **65**, 403-413.

[24] De Meyer G., Shapiro F., Vanderstichele H., Vanmechelen E., Engelborghs S., De Deyn P. P., Coart E., Hansson O., Minthon L., Zetterberg H., Blennow K., Shaw L., Trojanowski J. Q., Alzheimer's Disease Neuroimaging Initiative (2010) Diagnosis-independent Alzheimer disease biomarker signature in cognitively normal elderly people. *Arch Neurol* **67**, 949-956.

[25] Jack C. R., Jr., Knopman D. S., Chetelat G., Dickson D., Fagan A. M., Frisoni G. B., Jagust W., Mormino E. C., Petersen R. C., Sperling R. A., van der Flier W. M., Villemagne V. L., Visser P. J., Vos S. J. (2016) Suspected non-Alzheimer disease pathophysiology–concept and controversy. *Nat Rev Neurol* **12**, 117-124.

[26] Dale AM Fischl B, Sereno MI (1999) Cortical surface-based analysis. I. Segmentation and surface reconstruction. *Neuroimage* **9**, 179-194.

[27] Fischl B Sereno MI, Tootell RB, Dale AM (1999) High-resolution intersubject averaging and a coordinate system for the cortical surface. *Hum Brain Mapp* **8**, 272-284.

[28] Iglesias JE Sabuncu MR, Van Leemput K; Alzheimer's Disease Neuroimaging Initiative (2012) Incorporating parameter uncertainty in Bayesian segmentation models: application to hippocampal subfield volumetry. *Med Image Comput Comput Assist Interv* **15**, 50-57.

[29] Yendiki A Koldewyn K, Kakunoori S, Kanwisher N, Fischl B (2014) Spurious group differences due to head motion in a diffusion MRI study. *Neuroimage* **88**, 79-90.

[30] Behrens TE Berg HJ, Jbabdi S, Rushworth MF, Woolrich MW (2007) Probabilistic diffusion tractography with multiple fibre orientations: What can we gain? *Neuroimage* **34**, 144-155.

[31] Von Der Heide RJ Skipper LM, Klobusicky E, Olson IR (2013) Dissecting the uncinate fasciculus: disorders, controversies and a hypothesis. *Brain* **136**, 1692-1707.

[32] Rimol LM Botellero VL, Bjuland KJ, Løhaugen GCC, Lydersen S, Evensen KAI, Brubakk AM, Eikenes L, Indredavik MS, Martinussen M, Yendiki A, Håberg AK, Skranes J (2019) Reduced white matter fractional anisotropy mediates cortical thickening in adults born preterm with very low birthweight. *Neuroimage* **188**, 217-227.

[33] Delli Pizzi S Franciotti R Taylor JP, Esposito R, Tartaro A, Thomas A, Onofrj M, Bonanni L (2015) Structural Connectivity is Differently Altered in Dementia with Lewy Body and Alzheimer's Disease. *Front Aging Neurosci* **7**, 208.

[34] Amaral R.S., Park, M.T., Devenyi, G.A., Lynn, V., Pipitone, J., Winterburn, J., . . . Alzheimer’s Disease Neuroimaging, I (2016) Manual segmentation of the fornix, fimbria, and alveus on high-resolution 3T MRI: Application via fully-automated mapping of the human memory circuit white and grey matter in healthy and pathological aging. *Neuroimage*.

[35] Fortea J Vilaplana E, Alcolea D, Carmona-Iragui M, Sánchez-Saudinos MB, Sala I, Antón-Aguirre S, González S, Medrano S, Pegueroles J, Morenas E, Clarimón J, Blesa R, Lleó A; Alzheimer's Disease Neuroimaging Initiative (2014) Cerebrospinal fluid β-amyloid and phospho-tau biomarker interactions affecting brain structure in preclinical Alzheimer disease. *Ann Neurol* **76**, 223-230.

[36] Sjöbeck M Haglund M, Englund E (2006) White matter mapping in Alzheimer's disease: A neuropathological study. *Neurobiol Aging* **27**, 673-680.

[37] Kantarci K., Murray M. E., Schwarz C. G., Reid R. I., Przybelski S. A., Lesnick T., Zuk S. M., Raman M. R., Senjem M. L., Gunter J. L., Boeve B. F., Knopman D. S., Parisi J. E., Petersen R. C., Jack C. R., Jr., Dickson D. W. (2017) White-matter integrity on DTI and the pathologic staging of Alzheimer's disease. *Neurobiol Aging* **56**, 172-179.

[38] Kantarci K Schwarz CG, Reid RI, Przybelski SA, Lesnick TG, Zuk SM, Senjem ML, Gunter JL, Lowe V, Machulda MM, Knopman DS, Petersen RC, Jack CR Jr (2014) White matter integrity determined with diffusion tensor imaging in older adults without dementia: influence of amyloid load and neurodegeneration. *JAMA Neurol* **71**, 1547-1554.

[39] Cavanna AE Trimble MR. (2006) The precuneus: a review of its functional anatomy and behavioural correlates. *Brain* **129**, 564-583.

[40] SA Back (2014) Cerebral white and gray matter injury in newborns: new insights into pathophysiology and management. *Clin Perinatol* **41**, 1-24.

Figures

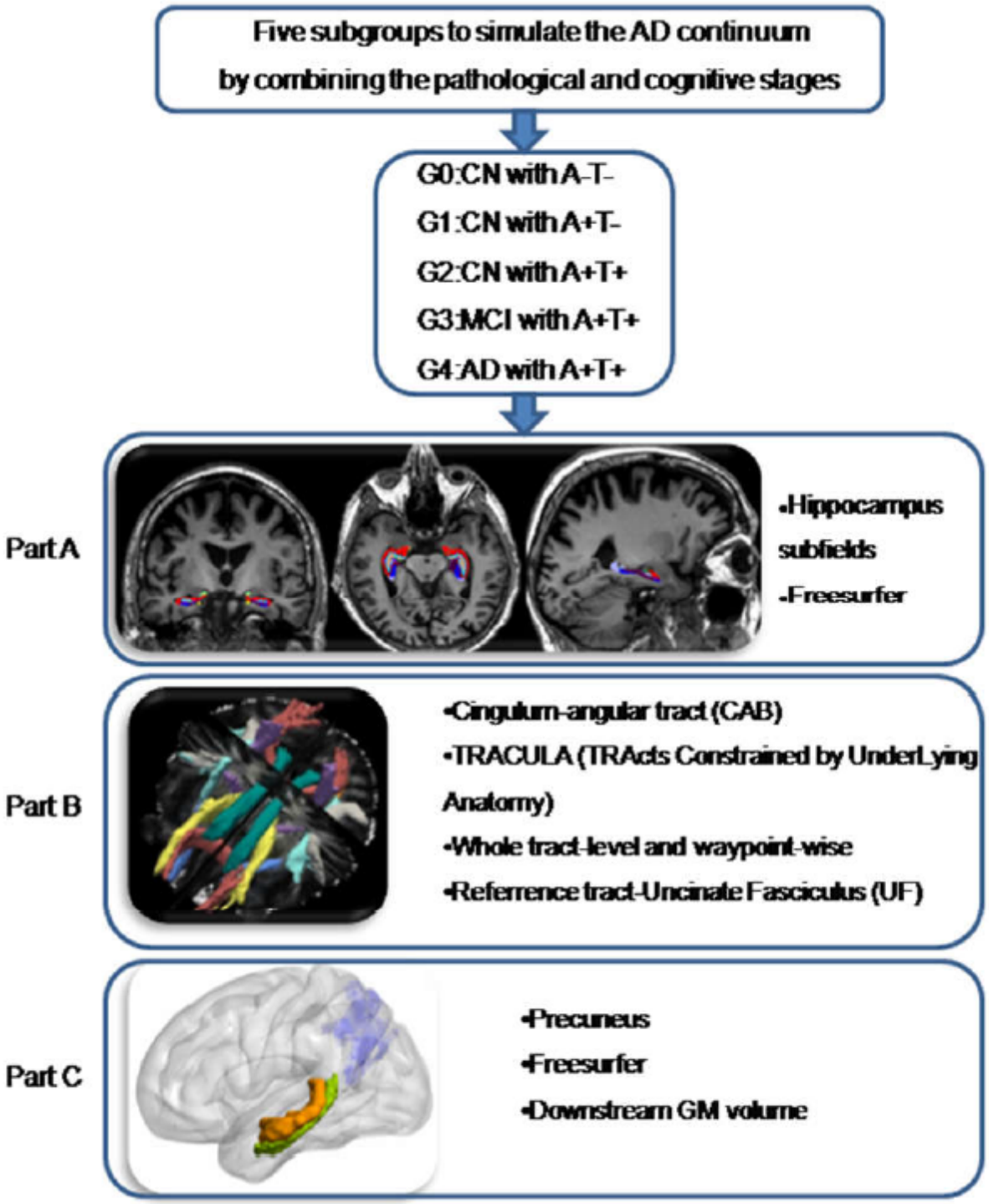

Figure 1

Image analysis path. Abbreviation: A: Aβ1-42; T: P-tau181; Group 0 (G0): cognitively normal subjects with A−T−; Group 1 (G1): cognitively normal subjects with A+T−; Group 2 (G2): cognitively normal subjects with A+T+; Group 3 (G3): mild cognitive impairment subjects with A+T+; Group 4 (G4): demented subjects with A+T+; HP: hippocampus; CA: cornu ammonis; GC-ML-DG: granule-cell molecular layer of the dentate gyrus; HATA: hippocampus-amygdala-transition-area

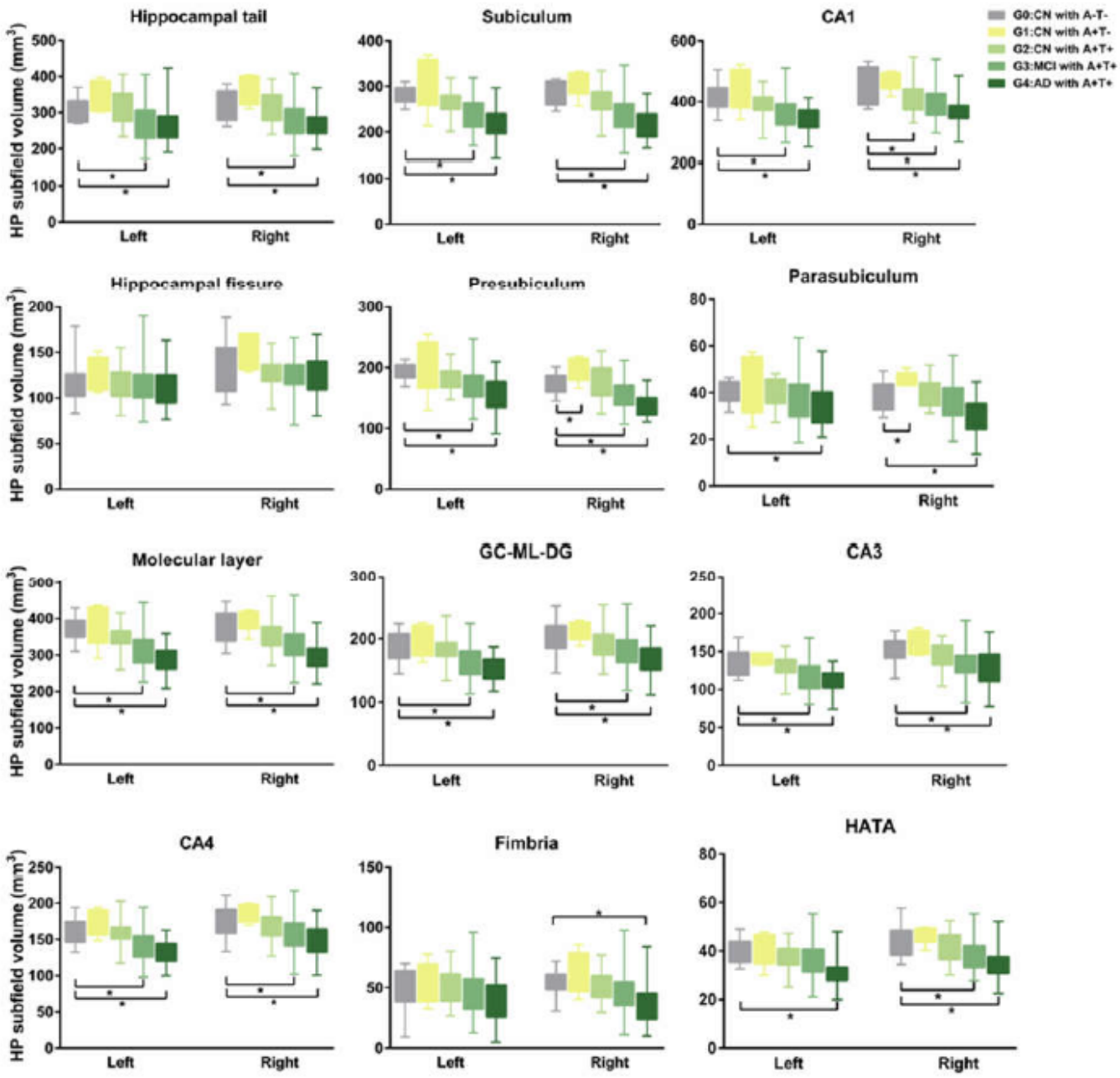

Figure 2

Comparison of HP subfields volume in G 0, 1, 2, 3 and 4. ∗P< 0.05. Abbreviation: A: Aβ1-42; T: P-tau181; Group 0 (G0): cognitively normal subjects with A−T−; Group 1 (G1): cognitively normal subjects with A+T−; Group 2 (G2): cognitively normal subjects with A+T+; Group 3 (G3): mild cognitive impairment subjects with A+T+; Group 4 (G4): demented subjects with A+T+; HP: hippocampus; CA: cornu ammonis; GC-ML-DG: granule-cell molecular layer of the dentate gyrus; HATA: hippocampus-amygdala-transition-area; CN: cognitively normal; MCI: mild cognitive impairment; AD: Alzheimer's disease

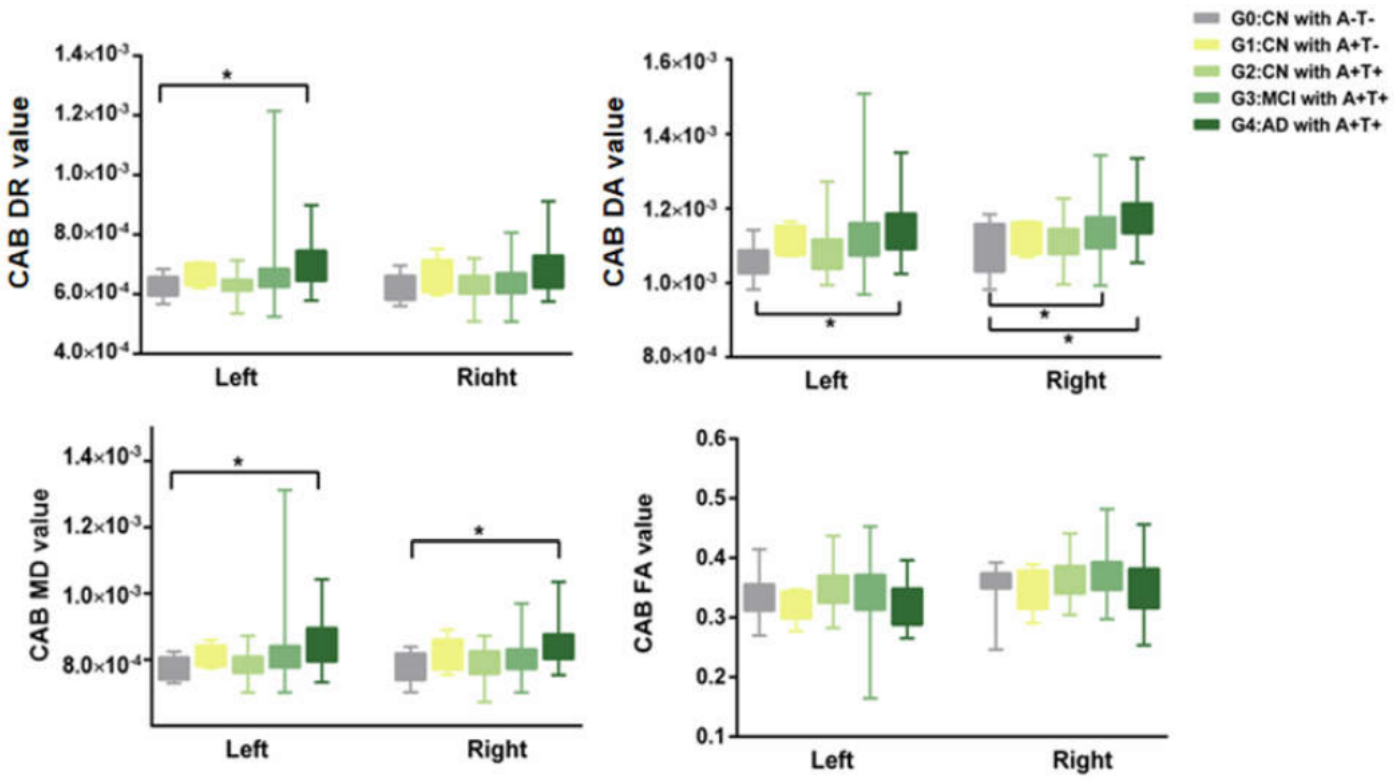

Figure 3

Comparison of averaged DA, DR, FA, MD in G 0, 1, 2, 3 and 4. ∗P< 0.05. Abbreviation: A: Aβ1-42; T: P-tau181; Group 0 (G0): cognitively normal subjects with A−T−; Group 1 (G1): cognitively normal subjects with A+T−; Group 2 (G2): cognitively normal subjects with A+T+; Group 3 (G3): mild cognitive impairment subjects with A+T+; Group 4 (G4): demented subjects with A+T+; CN: cognitively normal; MCI: mild cognitive impairment; AD: Alzheimer's disease; CAB: cingulum-angular bundles; DA: axial diffusivity; DR: radial diffusivity; FA: fractional anisotropy; MD: mean diffusivity;

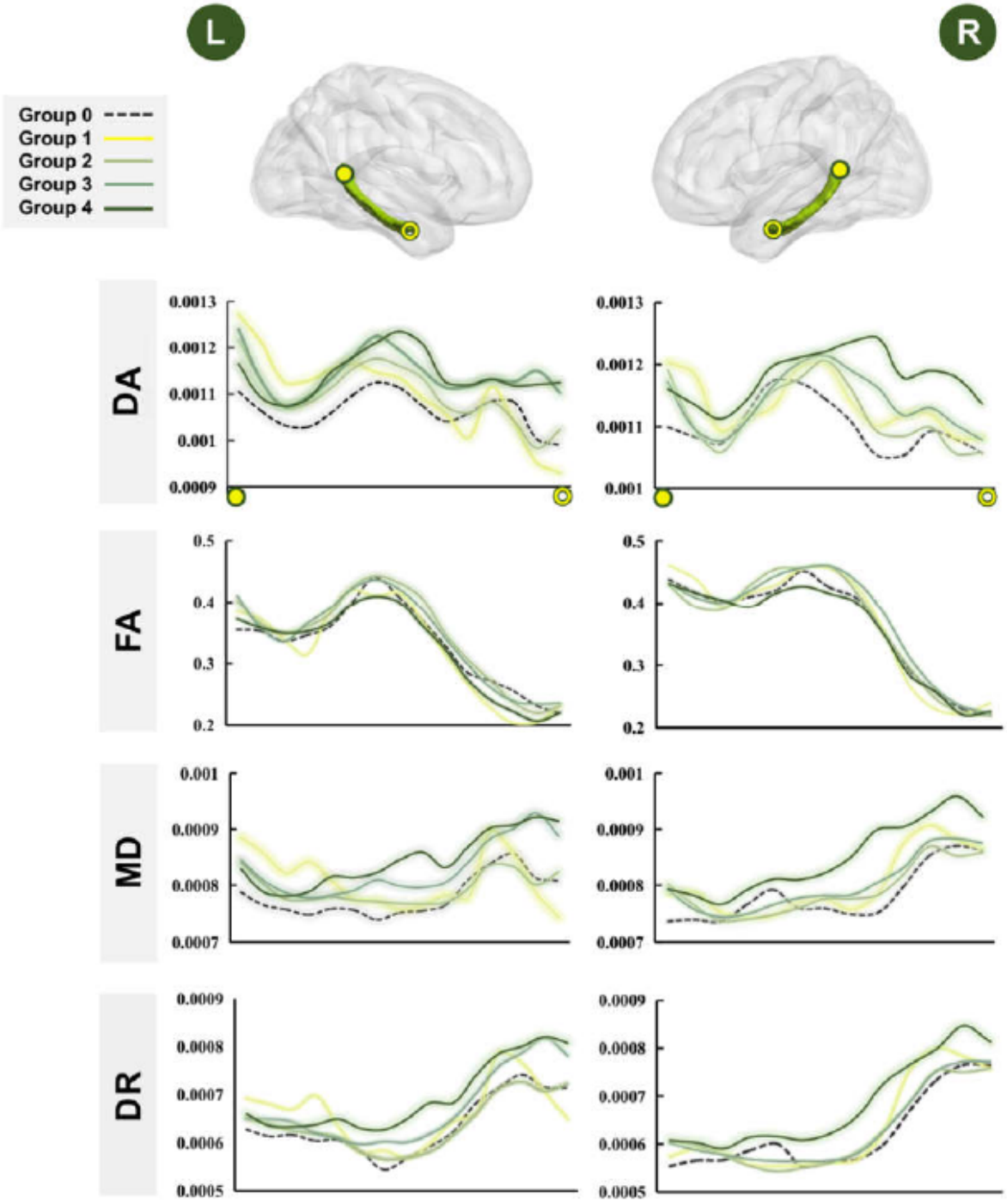

Figure 4

Diffusion metrics profiles of the selected tracts along AD continuum. The bilateral CAB were divided into 2.7 mm long segments in each subject's native space, and the average DA, FA, MD and DR value of each segment was obtained and mapped on each side. The x axis shows the location of the constructed tract from backward to forward (corresponding to yellow solid point and hollow point). Each line represents the group average diffusion metrics across subjects. Abbreviation: CAB, cingulum-angular bundles; DA, axial

diffusivity; FA, fractional anisotropy; MD, mean diffusivity; DR, radial diffusivity; A: Aβ1-42; T: P-tau181; Group 0: cognitively normal subjects with A−T−; Group 1: cognitively normal subjects with A+T−; Group 2: cognitively normal subjects with A+T+; Group 3: mild cognitive impairment subjects with A+T+; Group 4: demented subjects with A+T+;

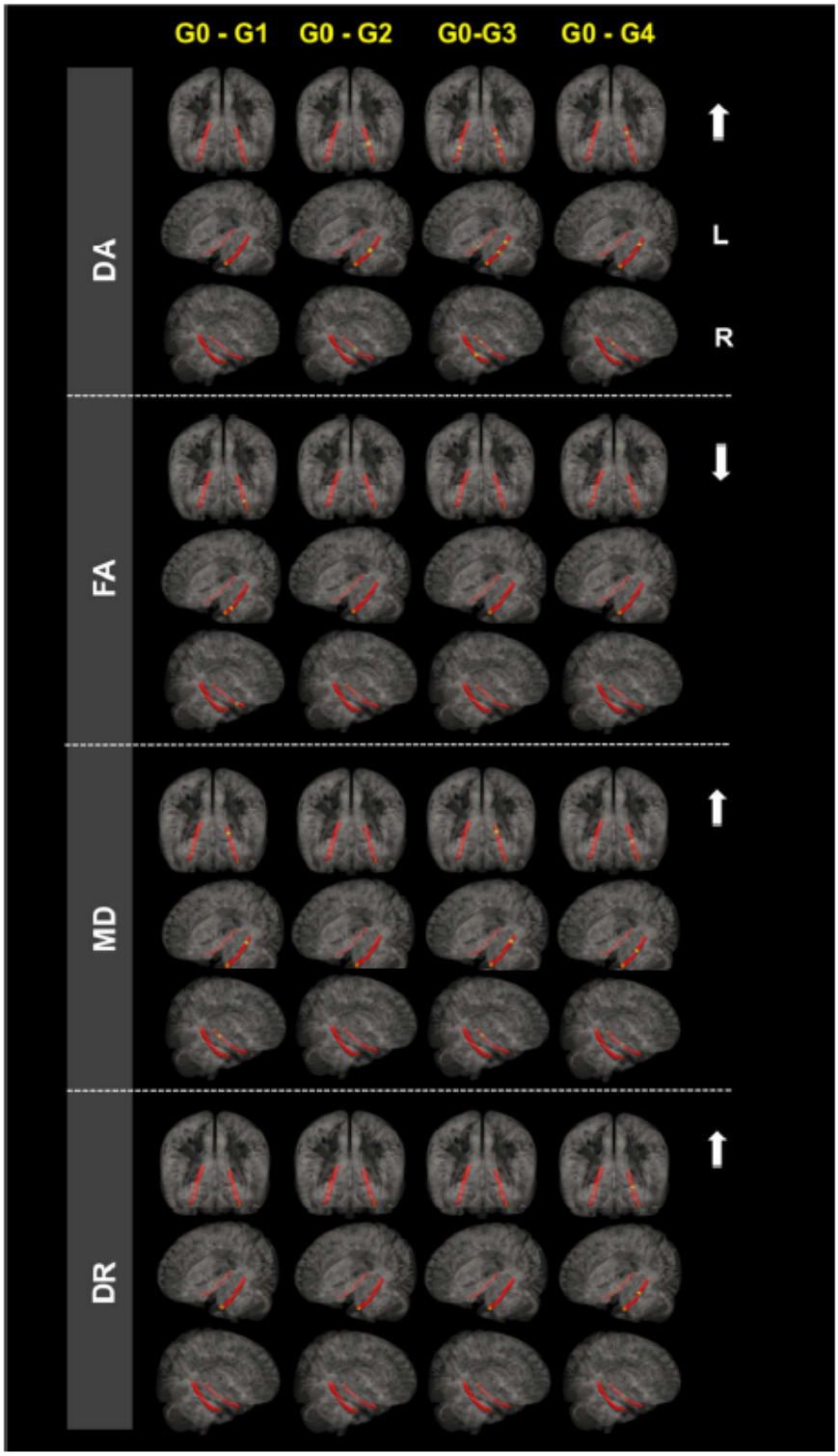

Figure 5

Waypoint-wise diffusion metrics analysis. The figure shows significance tests of group differences in DA, FA, MD and DR along left and right CAB. The result of each diffusion metric was displayed in a coronal position, left side and right side in radiological views from the top to bottom. The tracts were divided into 2.7 mm long segments in each subject's native space, and the average FA of each segment was obtained for analysis. The p-values are obtained from general linear models fitted for each segment along the tract, with FA, MD, DR and DA of each segment as the dependent variable, group as a categorical predictor, and age, gender, education, and the selected tract volume as co-variables. Red represents the selected tracts. Yellow segments show significant group difference ($p < 0.05$) over a contiguous segment greater than 0.81 cm along a given pathway. The arrows represent the increase or decrease of the diffusion metrics. Abbreviation: CAB, cingulum-angular bundles; DA, axial diffusivity; FA, fractional anisotropy; MD, mean diffusivity; DR, radial diffusivity; A: Aβ1-42; T: P-tau181; Group 0 (G0): cognitively normal subjects with A−T−; Group 1 (G1): cognitively normal subjects with A+T−; Group 2 (G2): cognitively normal subjects with A+T+; Group 3 (G3): mild cognitive impairment subjects with A+T+; Group 4 (G4): demented subjects with A+T+;

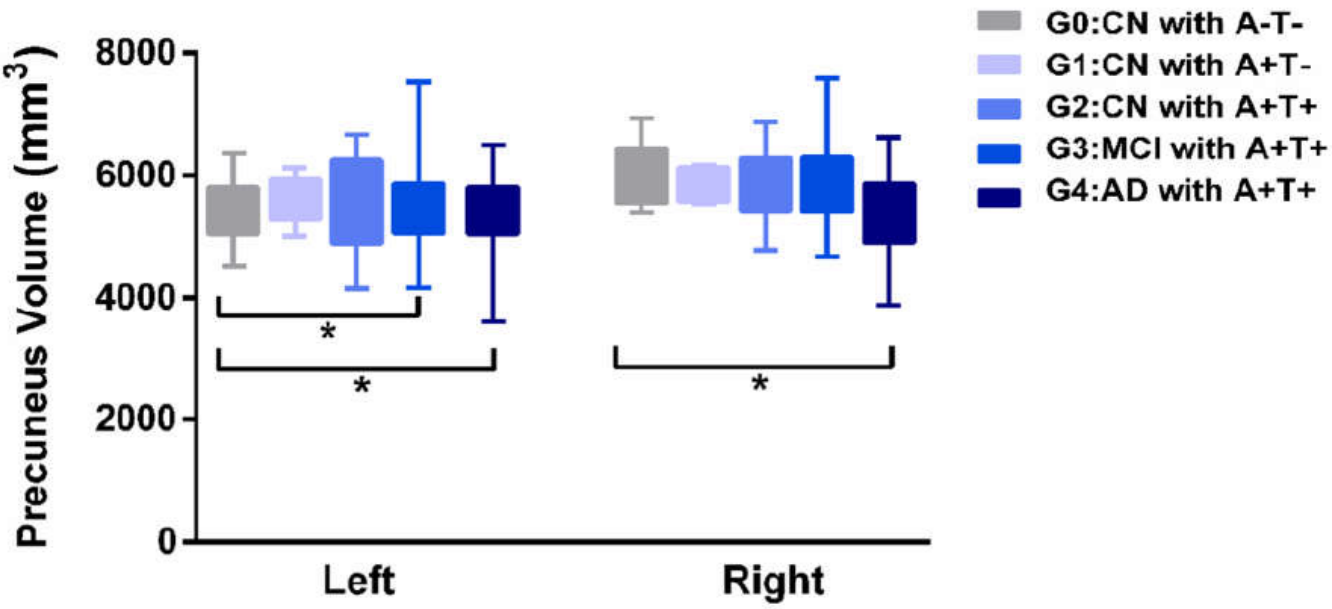

Figure 6

Comparison of precuneus volume between groups. ∗P< 0.05. Abbreviation: A: Aβ1-42; T: P-tau181; Group 0 (G0): cognitively normal subjects with A−T−; Group 1 (G1): cognitively normal subjects with A+T−; Group 2 (G2): cognitively normal subjects with A+T+; Group 3 (G3): mild cognitive impairment subjects with A+T+; Group 4 (G4): demented subjects with A+T+

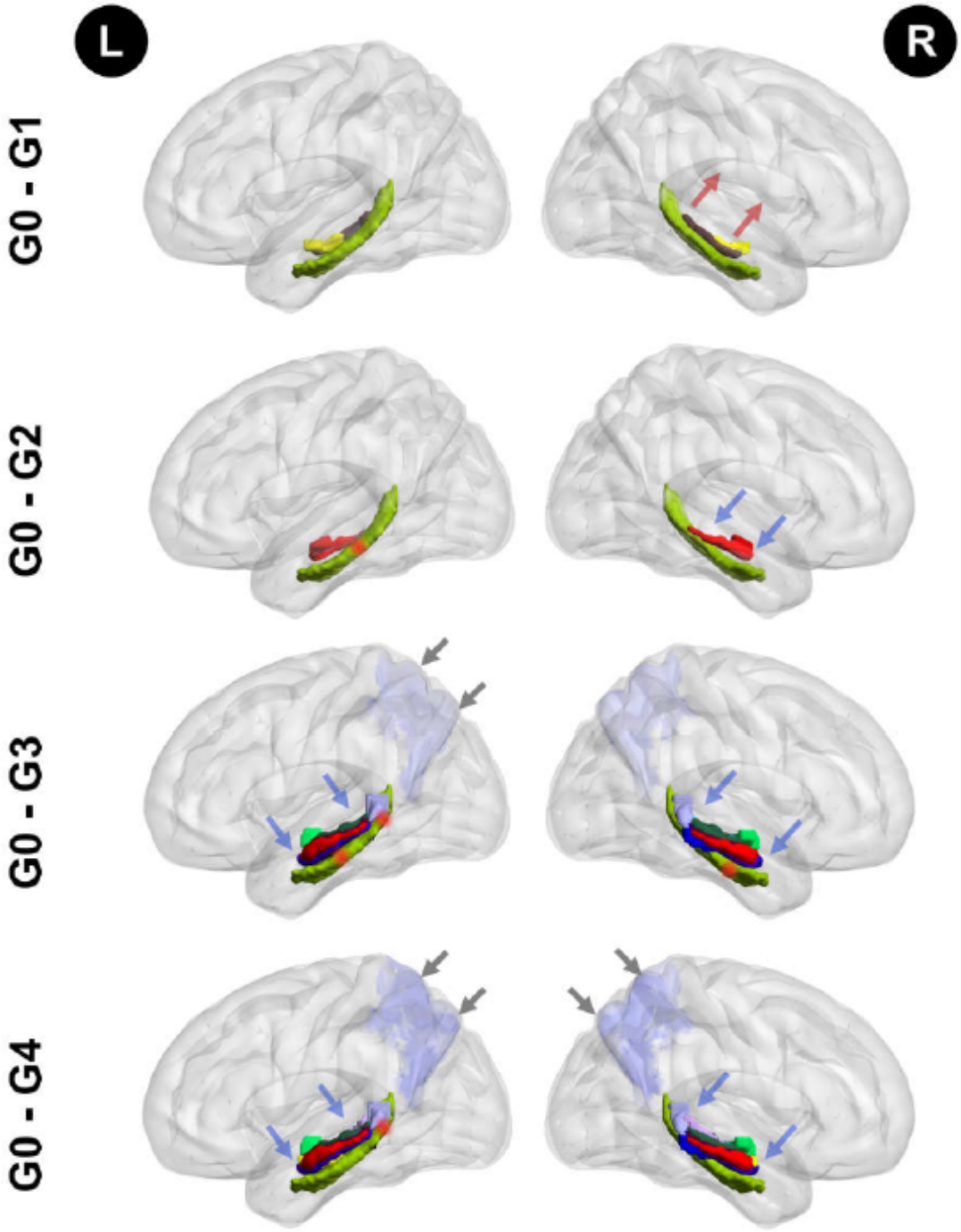

Figure 7

The impairments pattern of memory circuit structure along with Alzheimer's disease neuropathology spread. To show the results more clearly, we gathered all results to show the progressive impairments of memory circuit structure along with AD neuropathology spread. The green structure at the bottom represents the CAB tracts. Red segments of the CAB show significant group difference ($p < 0.05$) over a contiguous segment greater than 0.81 cm along a given pathway. The colourful structures above the

green structure represent the HP subfields. The lavender at the posterior brain region represents the precuneus volume. The arrows represent the decrease (blue) or increase (red) of the imaging metrics. In summary, when compared to G 0, G 1 showed larger right presubiculum and parasubiculum; G 2 showed smaller CA1; G 3 showed widespread decreased HP subfields volume, increased DA in right CAB, and decreased volume in the left precuneus; G 4 showed widespread decreased HP subfields volume, increased DA, DR and MD in the left CAB, increased DA and MD in the right CAB, and decreased volume in the bilateral precuneus. Abbreviation: AD: Alzheimer's disease; CAB, cingulum-angular bundles; A: Aβ1-42; T: P-tau181; Group 0 (G0): cognitively normal subjects with A−T−; Group 1 (G1): cognitively normal subjects with A+T−; Group 2 (G2): cognitively normal subjects with A+T+; Group 3 (G3): mild cognitive impairment subjects with A+T+; Group 4 (G4): demented subjects with A+T+; DA, axial diffusivity; MD, mean diffusivity; DR, radial diffusivity; HP: hippocampus

Supplementary Files

This is a list of supplementary files associated with this preprint. Click to download.

- Supplement.docx